Supplementary Information

Spontaneous thermal preserving and anti-gravitational water pumping Al_2O_3 fibers enhanced flexible nonwoven for high-performance and self-floating solar evaporator

Jiamu Dai[1], Hang Wang[1], Xiaochuan Yang[1], Liujia Lan[1], Suying Li[1], Yu Zhang[1], Rong Liu[1], Guangyu Zhang[1], Du Nie [2,*] and Wei Zhang[1,*]

[1] *School of Textile and Clothing, National & Local Joint Engineering Research Center of Technical Fiber Composites for Safety and Health, Nantong University, Nantong, 226001, China.*

[2] *College of Materials, Xiamen University, Xiamen, 361005, China.*

* Corresponding authors.

E-mail addresses: flory2114@hotmail.com (D. Nie), zhangwei@ntu.edu.cn (W. Zhang).

Experimental section

Materials and instruments

Al_2O_3 fibers (AOFs) were supplied by Chinese Academy of Sciences New Material Technology Co., Ltd. (Jiangsu, China). Kapok fibers (KFs) were obtained from Zhongshan Boflong Textile Co., Ltd. (Guangdong, China). Active carbon fiber felt (ACF, PAN-based) was obtained from Nantong Sen Carbon Fiber Co., Ltd. (Jiangsu, China). Waterborne polyurethane (WPU) was acquired from Jitian Chemical Co., Ltd. (Shenzhen, China). All chemicals involved were purchased from Sinopharm Chemical Reagent Co., Ltd. (Shanghai, China) without further purification.

Preparation of CuS particles

The CuS particles were prepared as description of the Reference [1]. Briefly, 0.5mmol

$Cu(CH_3COO)_2$ were firstly dissolved in 50ml DI water at 70℃ followed by dropwise adding NaOH solution to gain dark precipitate. After stirring for 5min, glucose was added as reducer to the above precipitate dispersion for another 20min stirring at 70℃ to prepare Cu_2O template. Afterwards, the dispersion was cooled down to room temperature and mixed with composite solution of Na_2S/ NaOH for 5min stirring to obtain CuS on the surface of the template. After centrifuging and washing with water and ethanol, the precipitate was separated and immersed in ammonia solution for 72h to remove unreacted Cu_2O. By further washing and freeze-drying, hollow-structured CuS particles were finally obtained.

Preparation of CuAAOK composite nonwoven materials

Firstly, AOFs and KFs were firstly carded separately to loosened mats, which were placed with ACFs felt as a sequence of ACFs-top, AOFs-middle and KFs-bottom for needle punching. The areal weight density is set as 2.2 $g \cdot dm^{-2}$ for ACFs, 0.3 $g \cdot dm^{-2}$ for AOFs and 0.6 $g \cdot dm^{-2}$ for KFs. The punching density and depth were set as 200-400 times/cm^2 and 9mm, respectively. Subsequently, the prepared CuS nanoparticles were dispersed in WPU emulsion with concentration of 100mg/30ml and then sprayed on the surface of ACFs with areal density of 180μl/cm^{-2}. After drying at room temperature, CuS coated composite nonwoven mat was prepared (marked as CuAAOK). In addition, needle punching samples without AOFs or CuS particles were also fabricated as control groups.

Characterizations

Morphological observation was obtained by field emission scanning electron microscope (FESEM, ZEISS Gemini SEM 300, Germany) and transmission electron microscope (TEM, FEI Talos F200X, USA). Hydrophilicity was tested on an automatic video micro contact angle measurement instrument (OCA40Micro, Dataphysics, Germany). Mechanical properties were measured through electronic universal testing machine (Instron 5969, USA). Infrared images were recorded by infrared camera (EXPEC 1810d, China). The absorbance spectra with wavelength from 200nm to 2500nm were gained from UV-vis-NIR scanning spectrophotometer (UV3600, Shimazu, Japan). FTIR spectra with wavenumber from 400cm^{-1} to 4000cm^{-1} were

determined using a spectrophotometer (Nicolet IS50, Thermo Scientific, USA). X-ray diffraction (XRD, D2 phaser, Bruker, Germany) was scanned from 10~80°. Water vapor transmission was analyzed by a Labthink W3-031 meter (China).

Porosity measurement

CuAAOK was cut into circle shape with diameter of 5cm, the thickness was also measured for apparent volume (V_0) calculation. Afterwards, CuAAOK was immersed in ethanol and stabilized for 10min to measure the volume increase of the system, then the actual volume (V) was obtained. Thus, the porosity of CuAAOK was calculated as $\varphi = (V_0 - V)/ V_0$.

Buoyancy analysis

KFs layer was stripped from the evaporator and measured for analyzing the relationship between punching density and self-floating ability as the following formulas:

$$W = F \quad (1)$$

$$W = (m_{CuAAOK} + m_{water}) \cdot g \quad (2)$$

$$F = \rho \cdot V \cdot g \quad (3)$$

$$V = S \cdot h \quad (4)$$

$$m_{CuAAOK} = \sigma \cdot S \quad (5)$$

where W is the weight of CuAAOK after adsorbing water, F is the buoyancy from the bulk water, m_{CuAAOK} is the mass of CuAAOK, m_{water} is the mass of water adsorbed by CuAAOK (3.46 times to m_{CuAAOK}, Figure S8), ρ is the density of water (1 g·cm^{-3}), V is the exclusion volume of CuAAOK to the water, g is the gravitational constant, S is the basal area of CuAAOK, h is the distance between the water level and CuAAOK bottom, σ is the areal density of CuAAOK (3.3 g·dm^{-2}).

Filtration

CuAAOK was cut into circle shape with appropriate diameter matching the inner wall of syringe and then inserted at the bottom to construct less sophisticated filtration system. Methylene blue (MB) solution was used again as wastewater for filtrating measurement and loaded in the vertically fixed filtration system. The filtrate was collected by glass bottle for further test.

Solar-driven steam generating measurement

All samples were cut into circle shape with diameter of 5cm for following investigation. The ambient temperature and humidity were maintained to 25℃ and 50%, respectively. Under irradiation of simulated solar system (CME-SL500, Microenergyc, China) containing AM 1.5G light filter, temperature changes in dry-condition of the two sides were both measured at the center position through thermocouples to analyze heat generation ability of photothermal agent by converting solar energy, as well as heat conductivity rate from top to bottom. The sensibility of heat generation was investigated by measuring surface temperature change when turning on/off irradiation for several cycles. For practical wet-condition, samples were placed onto the surface of simulated seawater (Cnsic Marine Biotechnology Co, Ltd, China) in a watch glass for temperature measuring. Due to the constant temperature of the interface between water and the bottom surface of samples, the middle position temperature was measured instead to reflect temperature change combining with top surface temperature when evaporating was processed under solar irradiation. In addition, the temperature change was also observed by thermal imaging camera (ONE-PRO, FLIR, USA).

For evaporation rate (ER) investigation, the mass change of sample covered simulated seawater was recorded by analytical balance (BSA224S-CW, Sartorius, Germany) under solar irradiation. The ER was calculated according to equation (6):

$$ER = \Delta m \,/\, (A \cdot t) \qquad (6)$$

where Δm is the mass change under light irradiation, A is the surface area of the evaporator, t is the irradiating time.

When measuring the ER in dark-condition, solar irradiation was removed. The vapor generated during solar irradiation was cooled to liquid and then collected through self-made glass cover with PMMA walls. For purification of wastewater, heavy metal ions solution containing Ca^{2+}, Ni^{2+}, Cu^{2+} and Mn^{2+} was prepared by dissolving equal concentration of $CaCl_2$, $NiCl_2$, $CuSO_4$ and $MnCl_2$ in DI water for testing purification ability under solar irradiation. The ion concentration of water before and after purification was tracked by ICP-OES (ICS5000+, Thermo Fisher, USA). The drinkable water standard of World Health Organization

(https://www.who.int/publications/i/item/9789240045064) was used to evaluate the quality of evaporated water. Likewise, MB solution (10mg/L) was also prepared as simulated pollutant for testing of organic wastewater purification by comparing the absorbance of UV-vis spectra before and after purification.

Anti-bacteria and cell viability experiments

For anti-bacteria experiment, *Escherichia coli* (*E. coli*) and *Staphylococcus aureus* (*S. aureus*) dispersions in cultural medium were sprayed on ACFs side of sanitized CuAAOK respectively. Afterwards, bacteria carried CuAAOK was irradiated by simulated sunlight with power of 1 sun for 10min under sterile condition. Phosphoric acid buffer solution (PBS) was used to repeatedly wash CuAAOK for 5 times. The recycled PBS was transferred onto agar in culture dish for following incubated under 37℃ for 24h in an incubator. For comparison, gauze was set as control group. In addition, the influence of irradiation was also considered. After incubation, culture dishes were taken out to observe the bacteria proliferation for analyzing the solar-driven anti-bacteria capacity of CuAAOK.

Fibroblast cells (L929) were used to cell viability experiments. Briefly, 5×10^3 cells per well were firstly seeded in 96-well plates and incubated for 12h with fetal bovine serum containing DMEM medium under condition of 37℃ and 5% CO_2. Afterwards, medium was removed and cells were washed with phosphate buffer solution (PBS) for three times. Subsequently, DEME medium prepared in advance by ultra-pure water or condensed water from evaporation of CuAAOK was used to culture cells for 48h. After removing medium and washing, 10 vt% MTT solution (5mg/mL) in FBS-free medium was added to each well for another 4h incubation. Next, the solution was replaced by 100μl dimethyl sulfoxide (DMSO). The plate was placed in a 37℃ and 100rpm shaker for 10min. Finally, the optical value of each well was read by a microplate reader (MK3, Thermo, USA) at wavelength of 492nm as presenting cell viability.

Supporting Videos

Movie S1: The salt particles dissolved by the transported water on the evaporator surface to reveal the salt resistance.

Fig. S1 Digital photograph of CuAAOK from ACFs and KFs sides.

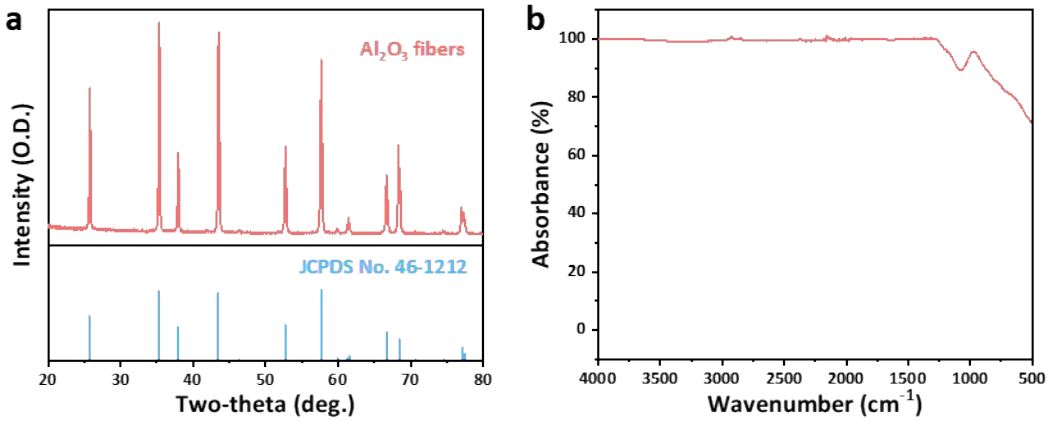

Fig. S2 Characterizations of AOFs. a) XRD spectrum. b) FTIR spectrum.

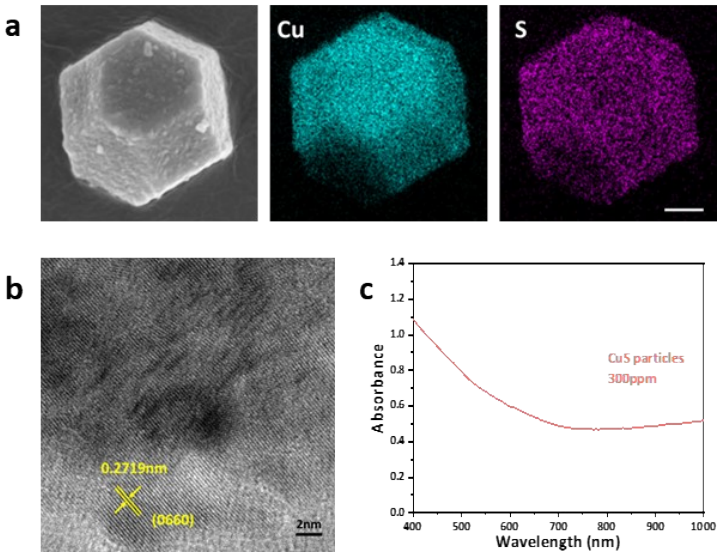

Fig. S3 Characterization of CuS particles. a) EDS mapping (scale bar=1.25μm), b) HRTEM pictures, c) UV-vis spectrum.

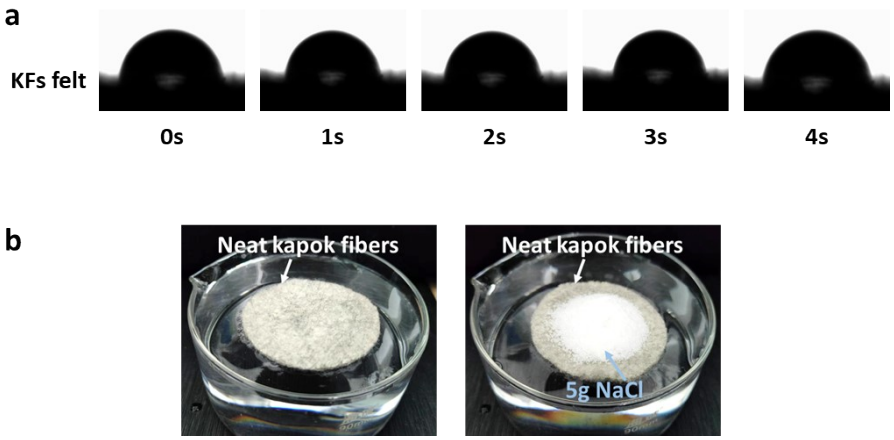

Fig. S4 Self-floating investigation of KFs. a) Water contact angle test of KFs felt. b) Digital photographs of neat kapok fibers felt with needle punching before and after adding 5g NaCl particles (sample diameter=5cm).

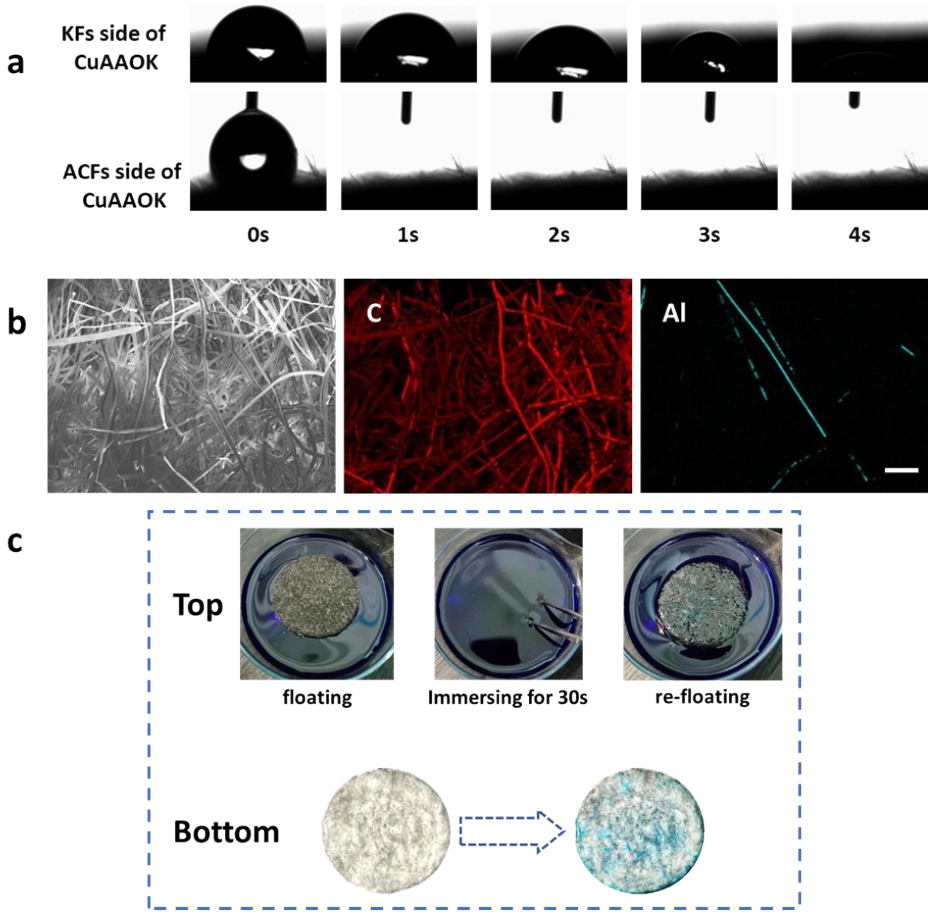

Fig. S5 Water transport analysis of CuAAOK. a) Water contact angle test of ACFs and KFs sides of CuAAOK. b) SEM and EDS mapping (C and Al) pictures of CuAAOK bottom (scale bar=250μm). c) Digital photographs of top and bottom observation before and after immersing under methylene blue solution for 30s (Sample diameter=5cm).

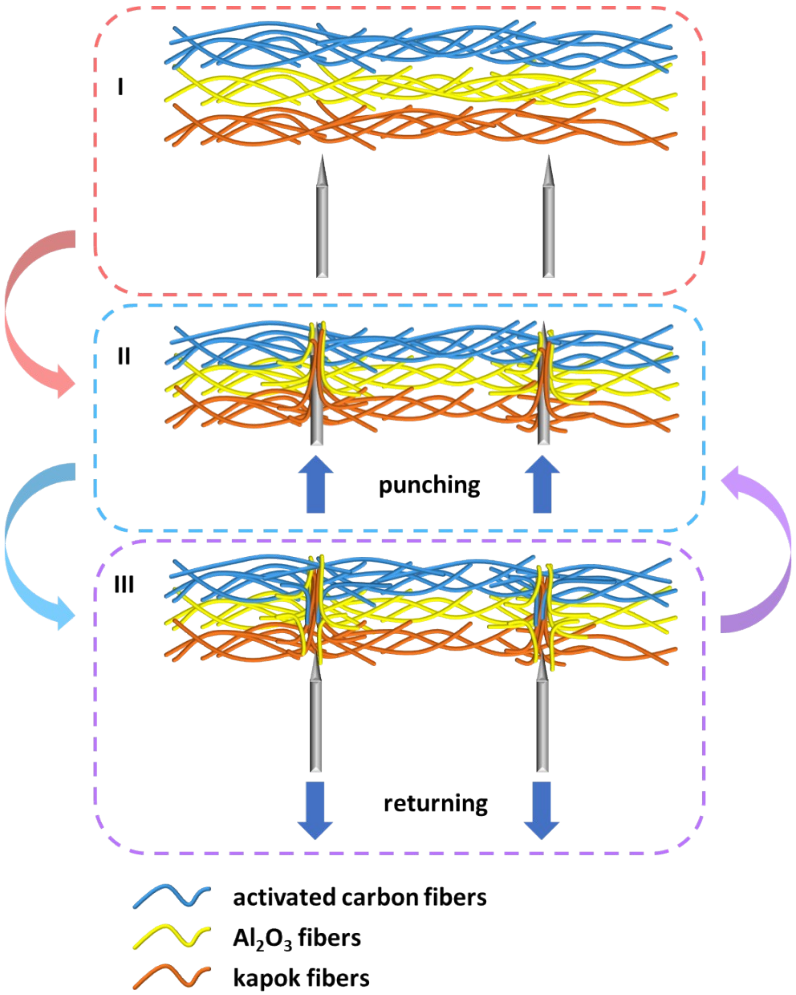

Fig. S6 Scheme of needle punching process on multi-layered nonwoven mat. I. carded fiber mats before needle punching. II. carded fiber mats with needle punching. III. needles returning back.

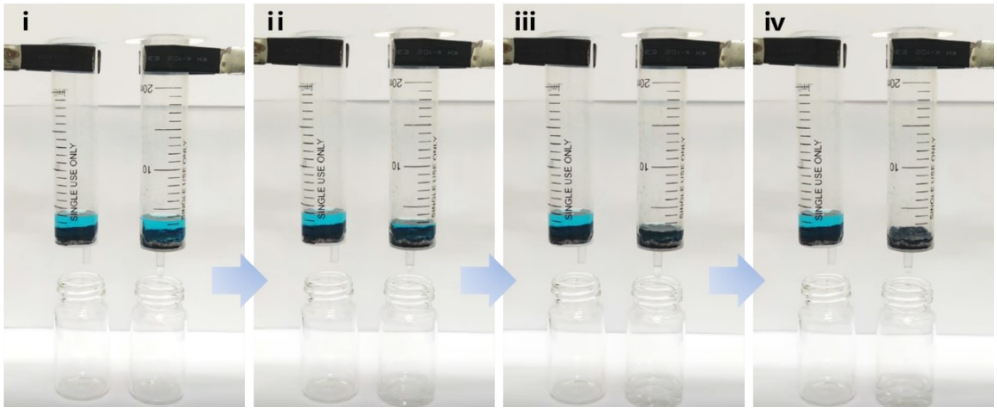

Fig. S7 MB solution transferring from ACFs side (left) and KFs side (right) of CuAAOK.

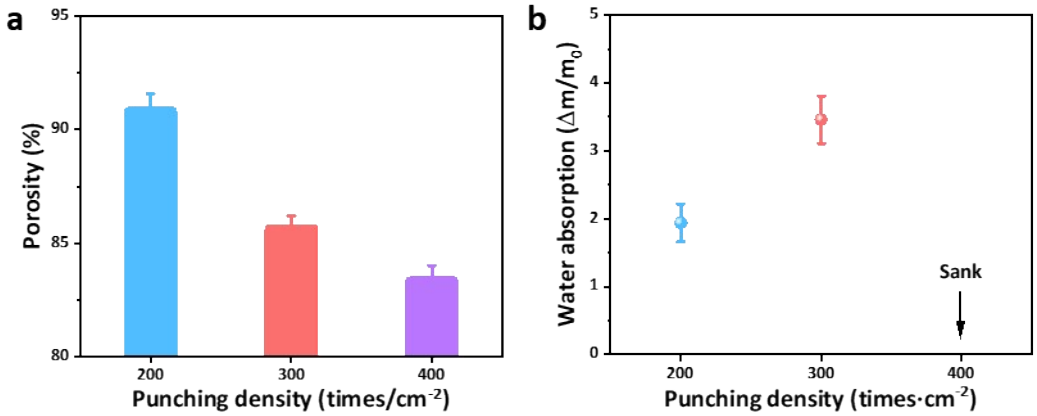

Fig. S8 Influence of punching density to self-floating ability of CuAAOK. a) Porosity of CuAAOK under different punching density. b) Water absorption of CuAAOK with different punching density after placed on the surface of simulated seawater for 30min.

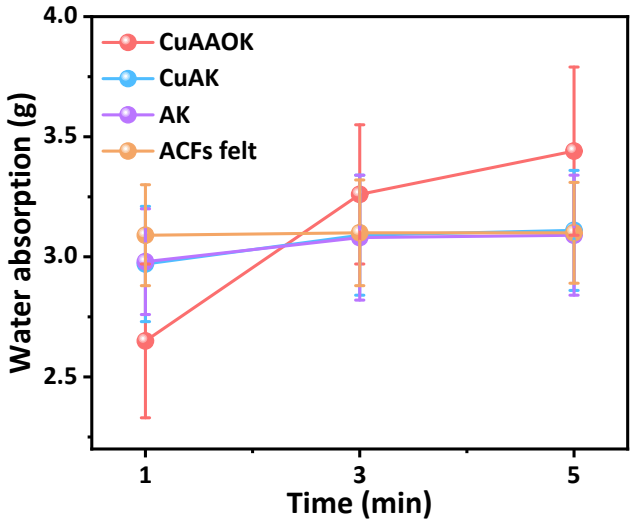

Fig. S9 Water absorption of ACFs felt, AK, CuAK and CuAAOK after placed on the surface of simulated seawater. (Sample diameter=5cm)

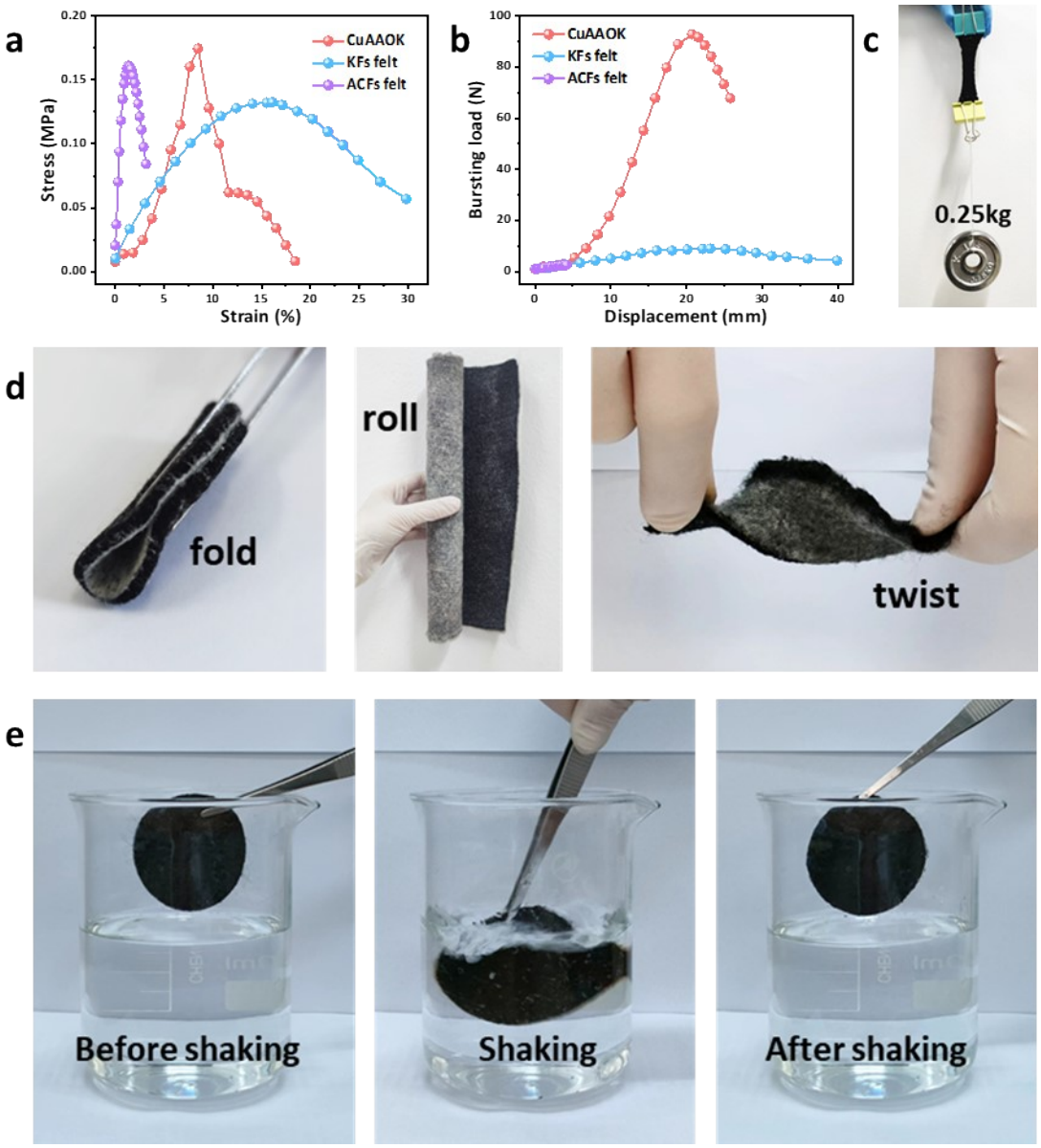

Fig. S10 Mechanical property investigation of CuAAOK. a) Tensile and b) bursting strength of CuAAOK. c) Digital photograph of CuAAOK with 0.25kg tension strength. d) Flexibility of CuAAOK after changing to different shapes. e) Digital photograph of CuAAOK before and after shaking in the water.

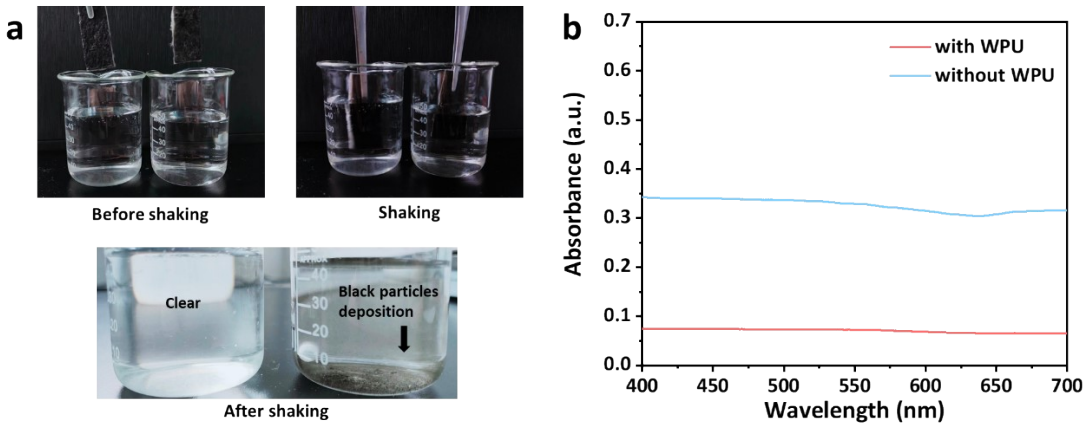

Fig. S11 a) Digital photograph of CuAAOK with (left) or without (right) WPU after shaking in the water. b) UV-vis spectra of washing water of CuAAOK with or without WPU.

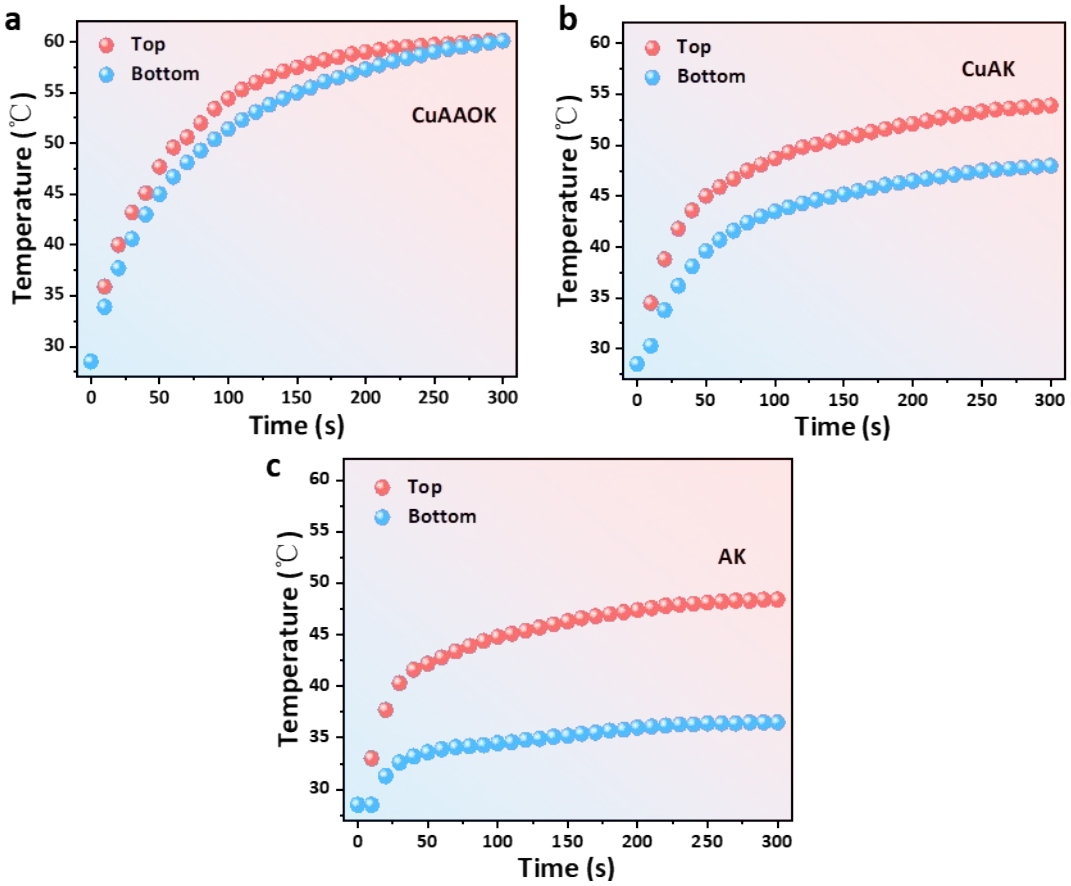

Fig. S12 Top and bottom temperature profiles of a) CuAAOK, b) CuAK and c) AK under solar flux of 0.4 sun.

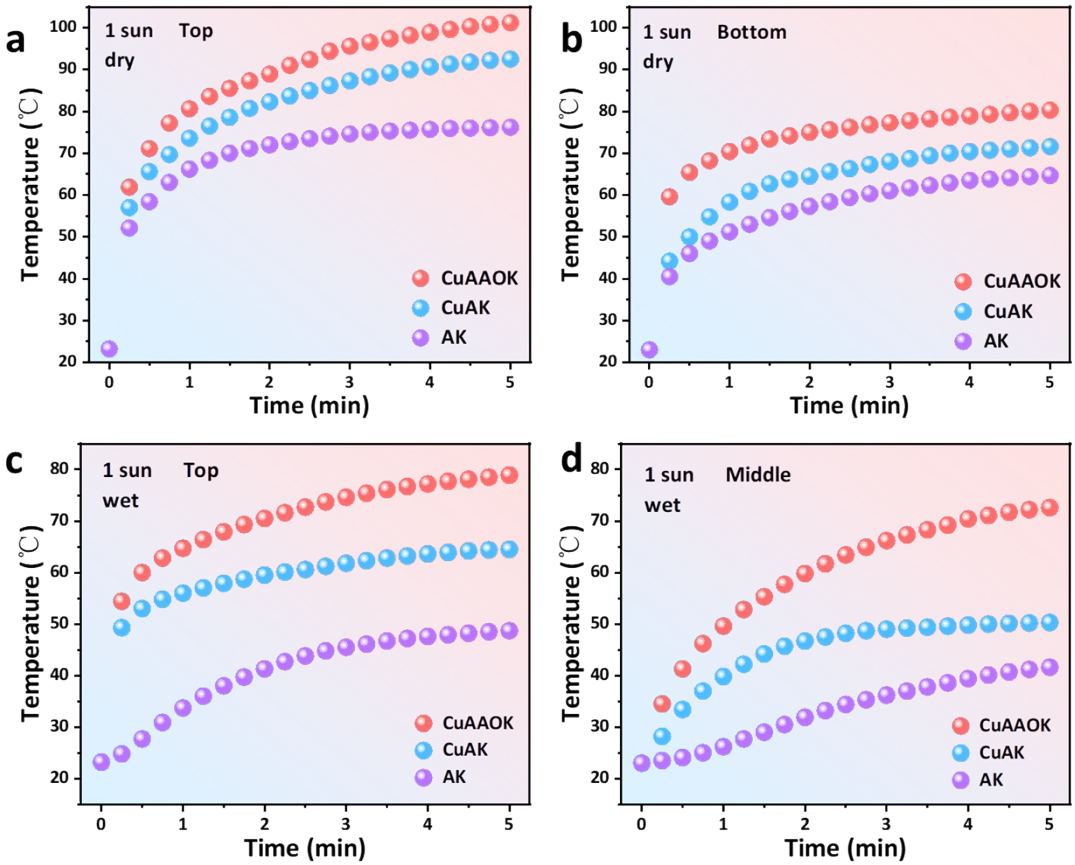

Fig. S13 Temperature profiles of CuAAOK, CuAK and AK under solar flux of 1 sun. a) top surface, dry condition. b) bottom surface, dry condition. c) top surface, wet condition. d) middle layer, wet condition.

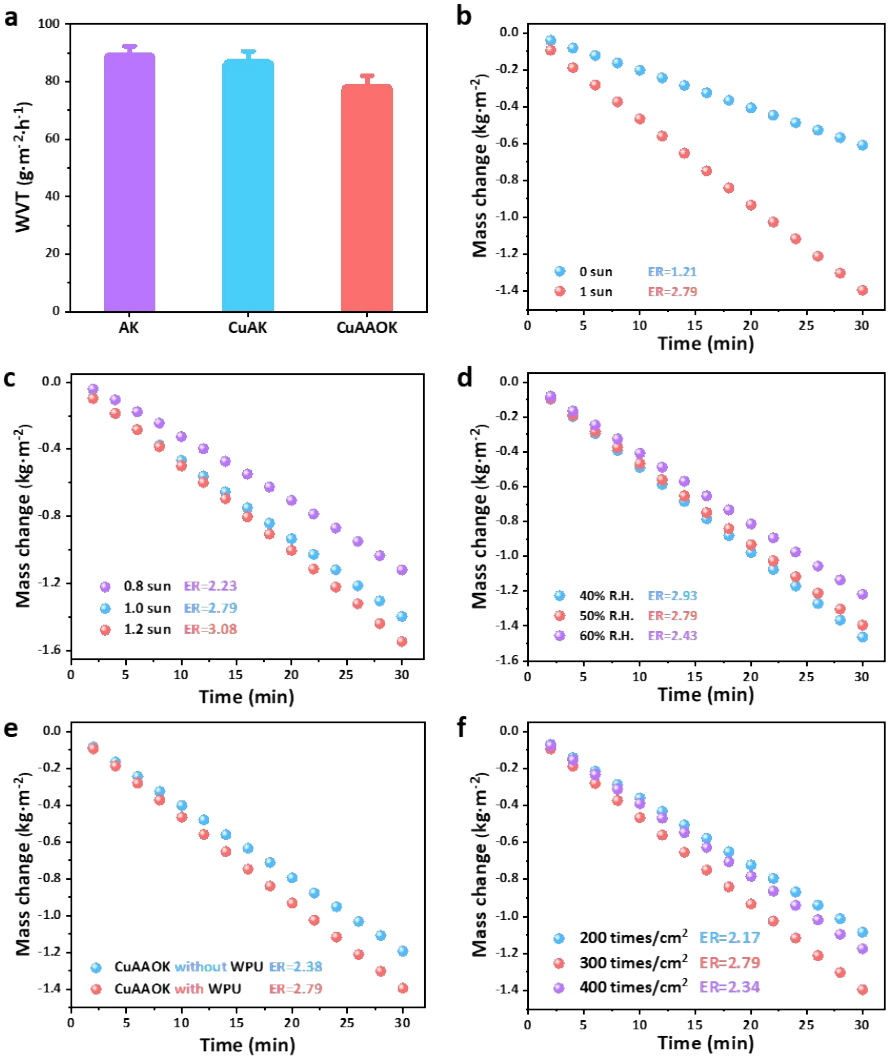

Fig. S14 Solar-driven evaporation investigation of CuAAOK. a) Water vapor transmission of CuAAOK, CuAK and AK. b) Evaporation rate profiles of CuAAOK with or without solar irradiation. c) Evaporation rate profiles of CuAAOK under 0.8, 1 and 1.2 sun illumination on simulated seawater. d) Evaporation rate profiles of CuAAOK under 30%, 40% and 50% relative humidity. e) Evaporation rate profiles of CuAAOK with or without WPU under 1 sun illumination on simulated seawater. f) Evaporation rate profiles of CuAAOK with different punching density (200, 300 and 400 times/cm^2).

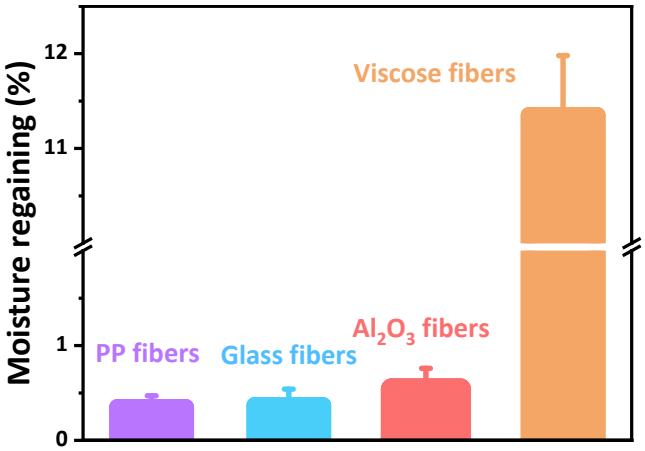

Fig. S15 Moisture regaining of PP, glass, Al_2O_3 and viscose fibers.

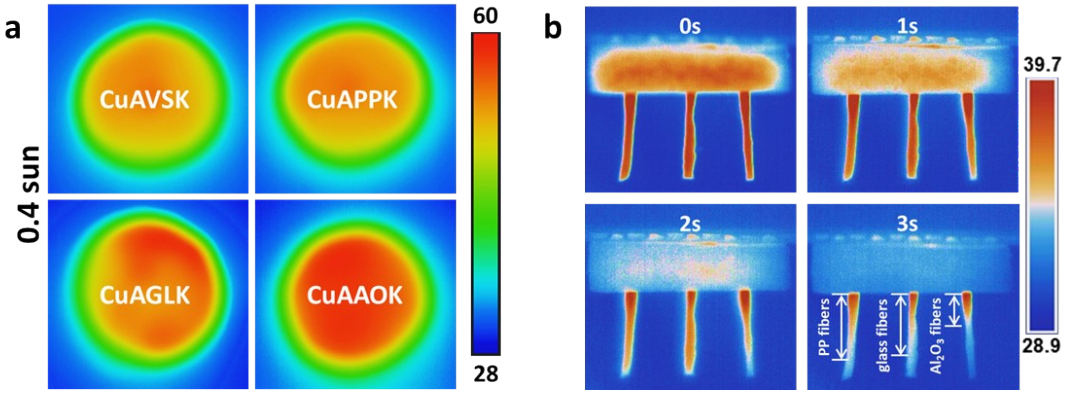

Fig. S16 Thermal management analysis of evaporators with different middle layer. a) Infrared thermal images of CuAAOK, CuAVSK, CuAPPK and CuAGLK under 0.4 sun illumination for 30min. b) Infrared images variation of PP, glass and Al_2O_3 fibers after heating to 40°C.

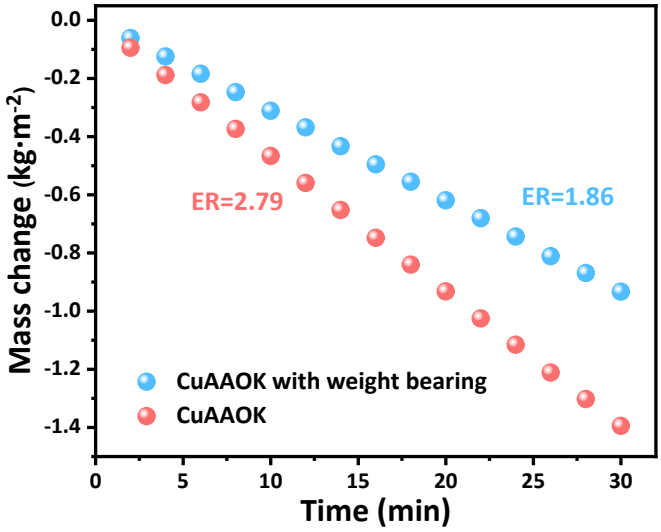

Fig. S17 Evaporation rate profiles of CuAAOK with or without weight bearing under 1 sun illumination on simulated seawater.

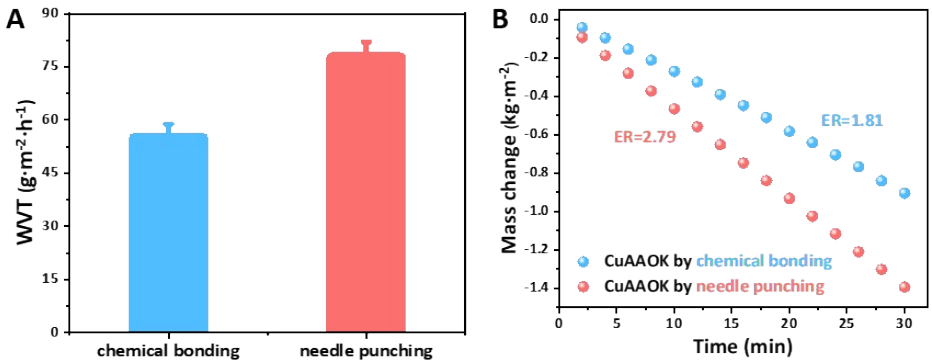

Fig. S18 Influence of fabrication methods on evaporation rate. a) Water vapor transmission of CuAAOK with chemical bonding and needle punching. b) Evaporation rate profiles of CuAAOK with chemical bonding and needle punching under 1 sun illumination on simulated seawater.

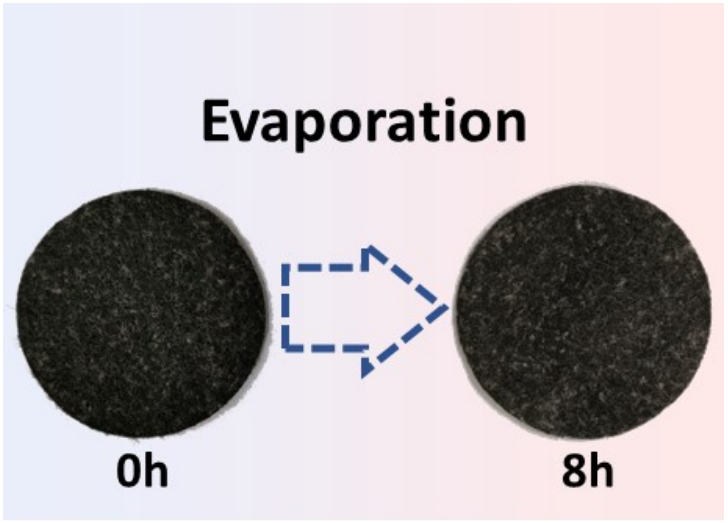

Fig. S19 Digital photograph of CuAAOK before and after evaporation.

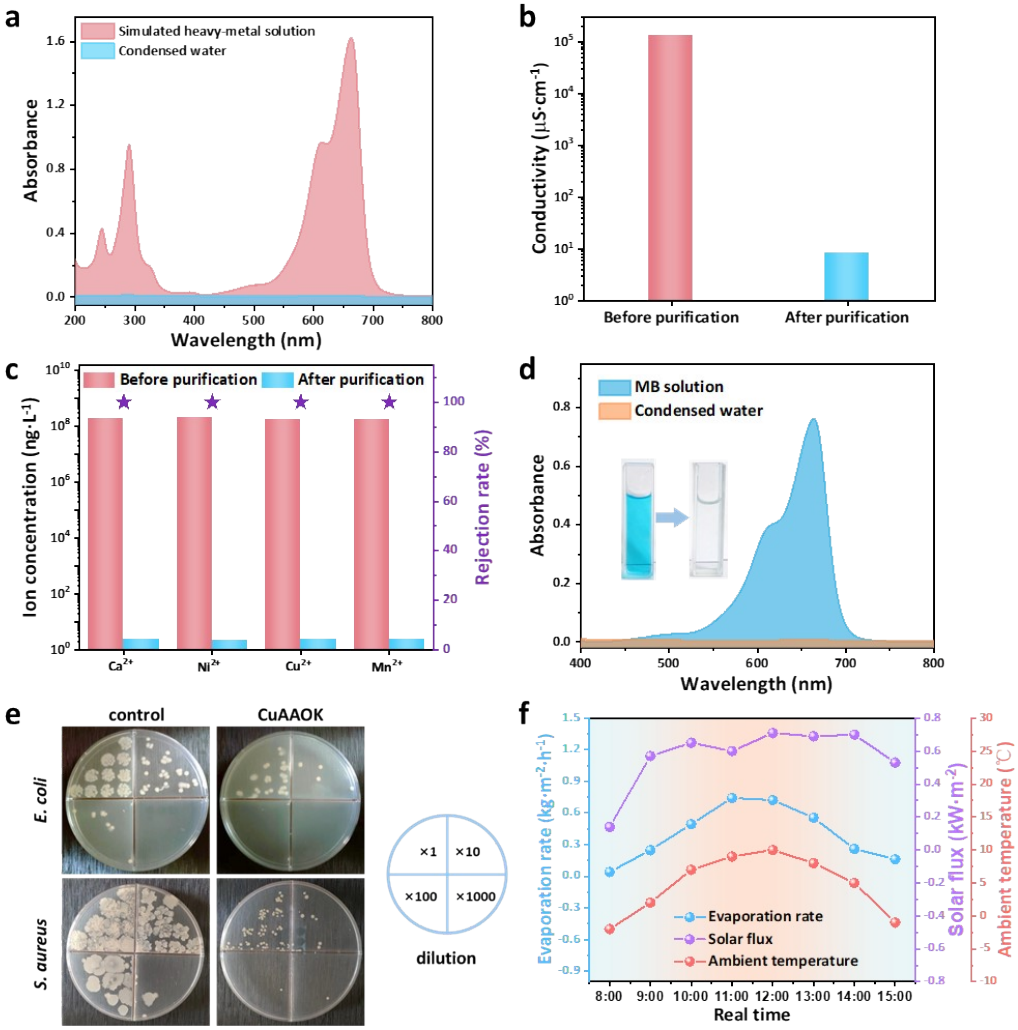

Fig. S20 Investigation of condensed water after evaporation. a) UV-vis spectra, b) conductive and c) ion concentration of simulated heavy metal wastewater before and after purification. d) UV-vis spectra and digital photographs (inserted pictures) of MB solution before and after purification. e) Digital photographs of anti-bacteria ability on control (gauze) and CuAAOK. f) Real-time variations of solar flux, ambient temperature and evaporation rate during winter outdoor experiment.

Table S1 Summary of solar-driven evaporators based on different materials in recent reports.

Materials	Method	Δm(kg/m²/h)	Refs
CuS/active carbon fibers/Al_2O_3 fibers/kapok fibers	**Needle punching**	**2.79**	**Current work**
SA/PVA/HACC hydrogel foam	sol–gel	**2.12**	**S2**
PDA/carbonized PVA/PVP hydrogel	freeze-dried/carbonization	**1.6**	**S3**
PVA/ PEDOT:PSS hydrogel	freezing dry	**2.5**	**S4**
CNT/PVDF-HFP	freezing dry	**2.35**	**S5**
rGO/PPy	hydrothermal	**1.44**	**S6**
Polypyrrole / airlaid paper	ice-templating	**1.38**	**S7**
ZrC/ filter paper	atomized and uniformly deposited	**1.38**	**S8**
PU /croconium dyes	coating	**1.272**	**S9**
CB/rGO/PS/Polysulfone	filtration	**1.86**	**S10**
PU/black paint	coating	**1.36**	**S11**
Nanocarbon/ PMMA/ cellulose acetate/ hemispheric polymeric foam	filtration	**1.43**	**S12**
Ni-MOF / carbon	coating	**2.07**	**S13**
CNT/silicon	sol–gel	**1.34**	**S14**
TiB_2-Ti/MoS_2	hydrothermal	**2.87**	**S15**
PS-cellulose-PDA-PPy-PDA spheres	coating	**2.6**	**S16**
PDA/PP mesh	coating	**1.645**	**S17**
chitosan/PAAm/PPy hydrogel	Thermal treatment	**2.41**	**S18**
CuS/PAN	electrospinning	**2.27**	**S19**
PSS/CNT/rGO	filtration	**1.825**	**S20**
CNT/glass fiber mesh	coating	**1.64**	**S21**

Supplemented references

S1. S. Sun, X. Song, C. Kong, S. Liang, B. Ding and Z. Yang, *CrystEngComm*, 2011, **13**, 6200-6205.

S2. N. Li, L. Luo, C. Guo, J. He, S. Wang, L. Yu, M. Wang, P. Murto and X. Xu, *Chemical Engineering Journal*, 2022, **431**, 134144.

S3. S. Chaule, J. Hwang, S.-J. Ha, J. Kang, J.-C. Yoon and J.-H. Jang, *Advanced Materials*, 2021, **33**, 2102649.

S4. N. Yang, F. Gong, B. Liu, Y. Hao, Y. Chao, H. Lei, X. Yang, Y. Gong, X. Wang, Z. Liu and L. Cheng, *Nature Communications*, 2022, **13**, 2336.

S5. B. Lv, C. Gao, Y. Xu, X. Fan, J. Xiao, Y. Liu and C. Song, *Desalination*, 2021, **510**, 115093.

S6. M. Zhang, F. Xu, W. Liu, Y. Hou, L. Su, X. Zhang, R. Zhang, L. Zhou, X. Yan, M. Wang, X. Hou and Y. Cao, *Nano Research*, 2022, DOI: 10.1007/s12274-021-4041-4.

S7. X. Wang, Q. Liu, S. Wu, B. Xu and H. Xu, *Advanced Materials*, 2019, **31**, 1807716.

S8. W. Zhou, C. Zhou, C. Deng, L. Chen, X. Zeng, Y. Zhang, L. Tan, B. Hu, S. Guo, L. Dong and S. C. Tan, *Advanced Functional Materials*, 2022, **32**, 2113264.

S9. G. Chen, J. Sun, Q. Peng, Q. Sun, G. Wang, Y. Cai, X. Gu, Z. Shuai and B. Z. Tang, *Advanced Materials*, 2020, **32**, 1908537.

S10. H. Fan, A. Gao, G. Zhang, S. Zhao, J. Cui and Y. Yan, *Chemical Engineering Journal*, 2021, **415**, 128798.

S11. L. Zhang, X. Li, Y. Zhong, A. Leroy, Z. Xu, L. Zhao and E. N. Wang, *Nature Communications*, 2022, **13**, 849.

S12. X. Zhou, P. Liu, W. Nie, C. Peng, T. Li, L. Qiang, C. He and J. Wang, *International Journal of Biological Macromolecules*, 2020, **149**, 116-126.

S13. P. He, L. Hao, N. Liu, H. Bai, R. Niu and J. Gong, *Chemical Engineering Journal*, 2021, **423**, 130268.

S14. C. Zhu, Z. Chen, R. Zhu, N. Sheng and Z. Rao, *Advanced Engineering Materials*, 2021, **23**, 2100327.

S15. R. Xu, H. Cui, K. Sun, X. Song, K. Yang, N. Wei, C. Hou and M. Zhao, *Chemical Engineering Journal*, 2022, **446**, 137275.

S16. X. Wu, Y. Wang, P. Wu, J. Zhao, Y. Lu, X. Yang and H. Xu, *Advanced Functional Materials*, 2021, **31**, 2102618.

S17. S.-L. Wu, L.-N. Quan, Y.-T. Huang, Y.-T. Li, H.-C. Yang and S. B. Darling, *ACS Applied Materials & Interfaces*, 2021, **13**, 39513-39522.

S18. T. Xu, Y. Xu, J. Wang, H. Lu, W. Liu and J. Wang, *Chemical Engineering Journal*, 2021, **415**, 128893.

S19. Z. Liu, Z. Zhou, N. Wu, R. Zhang, B. Zhu, H. Jin, Y. Zhang, M. Zhu and Z. Chen, *ACS Nano*, 2021, **15**, 13007-13018.

S20. Y. Wu, H. Huang, W. Zhou, C. You, H. Ye, J. Chen, S. Zang, J. Yun, X. Chen, L. Wang and Z. Yuan, *ACS Applied Materials & Interfaces*, 2022, **14**, 29099-29110.

S21. K. Yang, T. Pan, S. Dang, Q. Gan and Y. Han, *Nature Communications*, 2022, **13**, 6653.